WATER RESOURCES RESEARCH, VOL. 44, W09421, doi:10.1029/2007WR006639, 2008

Uniqueness and stability analysis of hydrogeophysical inversion for time-lapse ground-penetrating radar estimates of shallow soil hydraulic properties

Khan Zaib Jadoon,[1,2] Evert Slob,[3] Marnik Vanclooster,[2] Harry Vereecken,[1] and Sébastien Lambot[1,2]

Received 8 November 2007; revised 26 May 2008; accepted 20 June 2008; published 16 September 2008.

[1] Precise measurement of soil hydraulic properties at field scales is one of the prerequisites to simulate subsurface flow and transport processes, which is crucial in many research and engineering areas. In our study, we numerically analyze uniqueness and stability for integrated hydrogeophysical inversion of time-lapse, off-ground ground-penetrating radar (GPR) data in estimating the unsaturated soil hydraulic properties. In the inversion, hydrodynamic modeling based on the one-dimensional (1-D) Richards equation is used to physically constrain a full-waveform radar electromagnetic model. Synthetic GPR data, in terms of 3-D multilayered media Green's functions, were generated for three different textured soils (coarse, medium, and fine) and assuming different infiltration events. Inversion was performed iteratively to estimate three key soil hydraulic parameters (α, n, and K_s) of the Mualem-van Genuchten model using the global multilevel coordinate search optimization algorithm. For the coarse- and medium-textured soils, inversions converged to the actual solution for all scenarios. For the fine soil, estimation errors occurred, mainly because of the higher attenuation of the electromagnetic waves in such a soil (high electric conductivity). The procedure appeared to be generally stable with respect to possible errors in the hydrodynamic and petrophysical model parameterization. However, we found that particular attention should be given to an accurate estimation of the saturated water content and infiltration flux for real field applications. The results from our numerical experiments suggest that, in theory, the proposed method is promising for the noninvasive identification of the shallow soil hydraulic properties at the field scale with a high spatial resolution.

Citation: Jadoon, K. Z., E. Slob, M. Vanclooster, H. Vereecken, and S. Lambot (2008), Uniqueness and stability analysis of hydrogeophysical inversion for time-lapse ground-penetrating radar estimates of shallow soil hydraulic properties, *Water Resour. Res.*, *44*, W09421, doi:10.1029/2007WR006639.

1. Introduction

[2] Hydrological modeling is complicated by the relatively large spatiotemporal variability of the soil hydraulic properties at different scales, which mostly originates from the variations in soil texture and structure [*Ersahin and Brohi*, 2006], topography [*Brocca et al.*, 2007], ground temperature [*Behaegel et al.*, 2007], crop covers, and water redistribution by vegetation [*Hupet and Vanclooster*, 2002]. For instance, *Ersahin and Brohi* [2006] reported that the coefficient of variation for soil water content increased as soil water pressure decreased in both the topsoil (0–0.30 m) and subsoil (0.30–0.60 m), when sampled on a regular grid spacing of 25 m by 25 m. Cross dependence between sand content and soil water content showed that soil texture controlled the spatial variation of water content at the site, at all depths and pressures evaluated. However, the soil, which constitutes the interface between the aquifers and the atmosphere, plays a key role in hydrology as it supports key processes such as runoff, infiltration, evaporation and redistribution. In particular, field-scale knowledge of the soil hydraulic properties at spatiotemporal scales and resolutions that are relevant for the management of soil and water resources is essential for a wide range of environmental and agricultural applications.

[3] Gravimetric sampling and time domain reflectometry (TDR) are the principal methods used to characterize soil hydraulic properties at the local scale [*Robinson et al.*, 2003; *Heimovaara et al.*, 2004]. Each of these methods is time consuming, costly and provides only limited spatial coverage. At large scale (>100 m), airborne and spaceborne imagery can be useful to map soil water content [*Blumberg et al.*, 2000]. However, few robust methods are presently available to measure soil hydraulic properties at intermediate scales, ranging from 0.1–100 m, which are more pertinent to the water resources management, particularly in agriculture (e.g., farmland) [*Lunt et al.*, 2005]. In that respect, ground-penetrating radar (GPR) appears to be promising as a noninvasive method for characterizing and

[1]ICG-4 Agrosphere, Institute of Chemistry and Dynamics of the Geosphere, Forschungszentrum Jülich GmbH, Jülich, Germany.
[2]Department of Environmental Sciences and Land Use Planning, Université Catholique de Louvain, Louvain-la-Neuve, Belgium.
[3]Department of Geotechnology, Delft University of Technology, Delft, Netherlands.

0043-1397/08/2007WR006639$09.00

mapping the soil hydraulic properties at the field scale with a high spatial resolution. Recent reviews on the use of GPR in soil and hydrological sciences are given by *Huisman et al.* [2003] and *Annan* [2005].

[4] Time-lapse GPR is useful for retrieving soil hydraulic properties in the vadose zone [*Hubbard et al.*, 2005]. In particular, time-lapse GPR imaging can be used to characterize natural drainage inside the vadose zone [*Truss et al.*, 2007], for inverse multiphase flow simulations of dense nonaqueous phase liquid (DNAPL) migration [*Johnson and Poeter*, 2007], to monitor subsurface flow processes [*Tsoflias et al.*, 2001], or for water content estimation during irrigation and drainage [*Galagedara et al.*, 2005]. Cross-borehole GPR and travel time tomographic inversion techniques are widely used to monitor the distribution of water between boreholes and estimate key soil hydraulic properties using integrated or joint geophysical and hydrological inversion schemes [*Binley et al.*, 2002; *Rucker and Ferré*, 2004; *Kowalsky et al.*, 2005; *Cassiani and Binley*, 2005; *Linde et al.*, 2006; *Looms et al.*, 2008]. Off-ground GPR has also been used to monitor infiltration events in the laboratory and to derive the governing soil hydraulic properties using subsequent hydrodynamic inverse modeling [*Lambot et al.*, 2004a]. However, further developments and improvements are required in these methods to identify and map noninvasively the soil hydraulic properties at the field scale with a high spatial resolution. In that respect, *Lambot et al.* [2006a] recently proposed a new integrated inverse modeling approach to retrieve shallow subsurface hydraulic and electric profiles from time-lapse, off-ground GPR data. To reduce nonuniqueness in GPR data inversion, hydrodynamic modeling is used to limit the solution space to solutions obeying hydrodynamic laws. For a transient infiltration event in a sandy soil, the inverse solution was shown to be theoretically unique. This demonstrated that enough information may be contained in the time-lapse, off-ground radar data to estimate key soil hydraulic properties.

[5] In this paper, we extend the work of *Lambot et al.* [2006a] to three different soil textures, subject to different constant and variable flux rates. We investigate, using numerical experiments, the well posedness of the integrated inverse problem, in terms of uniqueness and stability of the inverse solution, to identify three key soil hydraulic parameters. The stability analysis focuses on the sensitivity of the inverse solution with respect to possible errors on the fixed hydraulic parameters, petrophysical models, and boundary and initial conditions in the hydrodynamic model. Such an analysis is in particular necessary to optimally parameterize the optimization procedure for solving the inverse problem with robustness and define the application range of the method. Numerical experiments also provide valuable insights into the effects of inversion choices; these insights would be difficult to gain from application to real field data, where the true moisture distribution is unknown. The effect of radar measurement errors on the inverse estimates is not investigated in this paper, as it requires a complete analysis including radar calibration, antenna transfer functions determination, and soil heterogeneity. Likewise, not all hydrodynamic modeling shortcomings that are likely to arise in real field applications are dealt with in this study (e.g., three-dimensional (3-D) flow, preferential flow, uniformity of the soil properties and boundary conditions, etc.). Future analysis will focus on real radar data sets for a more complete and realistic stability analysis.

2. Theory

2.1. Hydrogeophysical Inversion

[6] The hydrogeophysical inversion procedure analyzed in this paper, as depicted in Figure 1 [*Lambot et al.*, 2006a], applies to off-ground GPR for which accurate full waveform signal forward modeling is available, in terms of both phase (propagation time) and amplitude information [*Lambot et al.*, 2004c]. Nonuniqueness in retrieving continuous vertical water content profiles is overcome by constraining the classical electromagnetic inverse problem using soil hydrodynamic laws, thereby strongly reducing the possible solution space. The unknowns reduce to the soil hydraulic properties, denoted by vector **b** in Figure 1. The procedure requires knowledge of the hydrodynamic initial and boundary conditions and soil specific petrophysical relationships relating soil water content (θ) to soil electromagnetic properties, namely dielectric permittivity (ε) and electric conductivity (σ). We show in this paper that knowledge of the initial conditions may not be required. The measured and modeled time-lapse GPR data are represented by the 3-D GPR Green's functions $G_{xx}^{\uparrow}{}^{*}(f,t)$ and $G_{xx}^{\uparrow}(f,t,\mathbf{b})$, respectively. These are defined for wave propagation in multilayered media [*Michalski and Mosig*, 1997; *Slob and Fokkema*, 2002; *Lambot et al.*, 2004c], where f is the radar operating frequency and t is the time variable for the hydrodynamic event.

2.2. Hydrodynamic Model

[7] In this paper, we consider 1-D vertical water flow in a homogeneous and isotropic rigid porous medium whose hydrodynamics is described by Richards' equation, expressed here in terms of pressure head [*Jury et al.*, 1996]:

$$C(h)\frac{\partial h}{\partial t} = \frac{\partial}{\partial z}\left[K(\theta)\left(\frac{\partial h}{\partial z} - 1\right)\right] \tag{1}$$

where h is the time- and depth-dependent pressure head, $C(h) = \partial\theta(h)/\partial h$ is the differential water capacity with $\theta(h)$ being the water retention curve and θ being the volumetric water content, $K(\theta)$ is the hydraulic conductivity function, and z is the depth taken positive downward. For the case of infiltration under variable flux conditions, (1) is solved, subject to the following initial and boundary conditions:

$$h_i(z) = h_i(L) + z - L, \quad t = t_i, \quad 0 \le z \le L \tag{2a}$$

$$q(t) = K(\theta)\left(\frac{\partial h}{\partial z} - 1\right), \quad t \ge t_i, \quad z = 0 \tag{2b}$$

$$h(L^{+}) = 0, \quad h(L^{-}) = h(t), \quad t \ge t_i, \quad z = L \tag{2c}$$

which prescribe at the upper boundary the downward infiltration rate $q(t)$ (which may be negative for evaporation), and at the lower boundary a seepage face boundary condition, with L the soil column length. Subscript i stands for initial conditions ($t = t_i$).

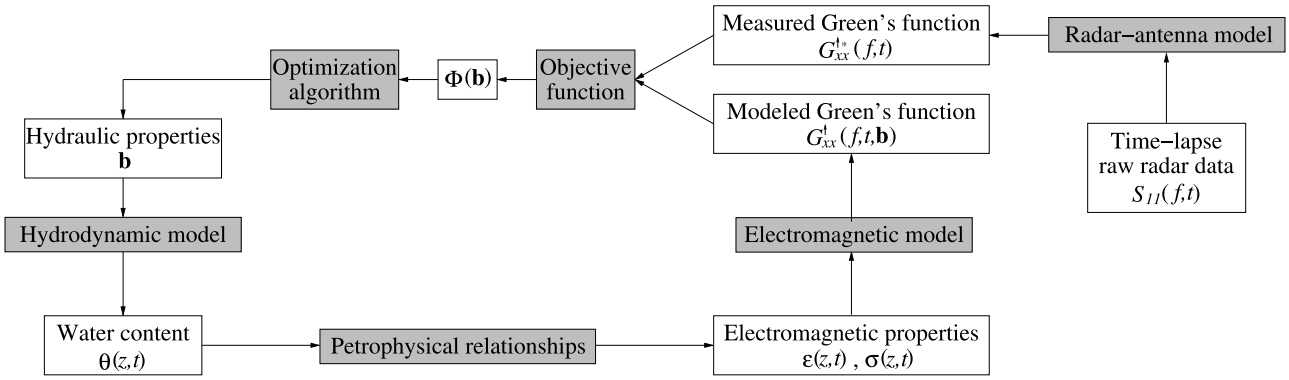

Figure 1. Flowchart representing the integrated electromagnetic and hydrodynamic inversion of time-lapse radar measurements for estimating soil hydraulic properties and electric profiles (t is time, z is depth, and f is frequency) [*Lambot et al.*, 2006a]. Shaded boxes denote operators, and white boxes denote variables.

[8] The classical Mualem-van Genuchten model (MVG) [*Mualem*, 1976; *van Genuchten*, 1980] is used in this study to describe the characteristic soil hydraulic properties. The water retention curve is given by

$$\theta(h) = \theta_r + (\theta_s - \theta_r)[1 + |\alpha h|^n]^{-m} \tag{3}$$

where θ_r and θ_s are, respectively, the residual and saturated water contents, α and n are curve shape parameters which are, respectively, inversely related to the air entry pressure value and the width of the pore size distribution, and m is restricted by the Mualem condition $m = 1 - 1/n$ with $n > 1$. The hydraulic conductivity relationship is given by

$$K(\theta) = K_s \left(\frac{\theta - \theta_r}{\theta_s - \theta_r}\right)^l \left[1 - \left(1 - \left(\frac{\theta - \theta_r}{\theta_s - \theta_r}\right)^{\frac{1}{m}}\right)^m\right]^2 \tag{4}$$

where K_s is the saturated hydraulic conductivity and l is a factor that accounts for the pore tortuosity.

[9] The total number of hydraulic parameters in the MVG model is six, i.e., θ_r, θ_s, α and n for the water retention curve, plus K_s and l for the unsaturated hydraulic conductivity function. Parameter θ_r is usually defined as the residual water content corresponding to a value of $h \rightarrow -\infty$. Generally, this parameter is regarded as an empirical parameter and can be fixed either to a value which yields the best fit to the experimental water retention data [*Kool et al.*, 1985], or to the value of zero [*Nimmo*, 1991; *Fuentes et al.*, 1992]. When considered different from zero, θ_r can be quite accurately inferred from soil texture using pedotransfer functions [*Vereecken et al.*, 1989] or directly derived from radar measurements under extremely dry conditions at the soil surface [*Lambot et al.*, 2006b]. Similarly, θ_s can be directly obtained from radar measurements when the soil surface is saturated [*Lambot et al.*, 2006b]. Parameter l is generally considered to have a small effect on the hydrodynamic events and can be either fixed to the average value of 0.5 or, preferably, estimated from bulk density and hydraulic conductivity with which it is highly correlated [*Vereecken*, 1995; *Lambot et al.*, 2002]. Given these considerations, we assumed θ_r, θ_s, and l to be known in the hydrogeophysical inversion process. The resulting parameter vector to be estimated is then defined as $\mathbf{b} = [\alpha, n, K_s]$.

2.3. Electromagnetic Model

[10] The electromagnetic model describing GPR wave propagation in the radar-antenna-air-soil system is described in detail by *Lambot et al.* [2004c] and *Lopera et al.* [2007]. It applies to ultrawideband stepped-frequency continuous wave radar combined with an off-ground monostatic transverse electromagnetic horn antenna. The radar system is based on international standard vector network analyzer technology. The raw radar data consist of the frequency-dependent complex ratio $S_{11}(\omega)$ between the backscattered field ($b(\omega)$) and the incident field ($a(\omega)$), ω being the angular frequency. Assuming the distribution of the electromagnetic field measured by the antenna to be independent of the soil properties, i.e., only the phase and amplitude of the field change, the antenna can be modeled using the following equation:

$$S_{11}(\omega) = \frac{b(\omega)}{a(\omega)} = H_i(\omega) + \frac{H(\omega) G_{xx}^{\uparrow}(\omega)}{1 - H_f(\omega) G_{xx}^{\uparrow}(\omega)} \tag{5}$$

where $H_i(\omega)$, $H(\omega)$, and $H_f(\omega)$ are the characteristic antenna transfer functions accounting for antenna propagation effects and antenna-soil interactions. The transfer functions $H_i(\omega)$ and $H_f(\omega)$ play the role of global reflectances, whereas $H(\omega)$ represents global transmitting and receiving transmittances. $G_{xx}^{\uparrow}(\omega)$ is the transfer Green's function of the air-subsurface system modeled as a 3-D multilayered medium. We define the Green's function as the backscattered x-directed electric field (upward component) at the antenna phase center for a unit x-directed electric source situated also at the antenna phase center. A distributed source may be used to account for the radiation pattern of the antenna compared to a dipole. A fine discretization of the multilayered medium compared to the minimal wavelength is used to represent continuously variable media (see below). The Green's function is derived using a recursive scheme to compute the global reflection coefficients of the multilayered medium in the spectral domain [*Born and Wolf*, 1980; *Michalski and Mosig*, 1997; *Slob and Fokkema*, 2002; *Lambot et al.*, 2004c]. The transformation back to the spatial domain is

Table 1. Mualem-Van Genuchten Hydraulic and Rhoades Petrophysical Parameters for the Three Textured Soils[a]

	Coarse	Medium	Fine
Hydraulic Parameters			
θ_r	0.025	0.010	0.010
θ_s	0.403	0.439	0.520
α (1/cm)	0.0383	0.0314	0.0367
n	1.3774	1.1804	1.1012
K_s (cm/min)	0.0417	0.0084	0.0172
l	1.2500	−2.3421	−1.9772
Petrophysical Parameters			
a	1.85	2.10	1.35
b	0.0385	0.2450	−0.0900
σ_s (S/m)	5.89e-4	8.99e-4	4.39e-2

[a]Mualem-Van Genuchten hydraulic parameters were obtained from HYPRES [*Wösten et al.*, 1999], and Rhoades petrophysical parameters were obtained from *Rhoades et al.* [1990].

performed by evaluating numerically a semi-infinite integral, for which a fast procedure has been developed [*Lambot et al.*, 2007].

[11] The constitutive parameters governing electromagnetic wave propagation are the dielectric permittivity ε (Fm^{-1}), electric conductivity σ (Sm^{-1}), and magnetic permeability μ (Hm^{-1}). In this paper, we assume μ equal to the permeability of free space, namely, $\mu_0 = 4\pi \times 10^{-7}$ Hm^{-1}, which is valid for non magnetic soil materials prevalent in most environments. The relative dielectric permittivity is defined as $\varepsilon_r = \varepsilon/\varepsilon_0$, where $\varepsilon_0 = 1/(\mu_0 c_0^2)$ is the dielectric permittivity of free space, with $c_0 = 299792458$ ms^{-1} being the speed of light in free space.

2.4. Petrophysical Relationships

[12] Numerous empirical and conceptual models exist to relate soil dielectric permittivity to volumetric water content, which are highly correlated because of the overwhelming dielectric properties of water compared to other soil constituents. For instance, the equation proposed by *Topp et al.* [1980] is generally used for a wide range of soils and water contents [*Kelleners et al.*, 2005], although it shows relatively large uncertainties in the low water content range and for soils with high clay or organic contents [*Dirksen and Dasberg*, 1993; *Heimovaara*, 1994]. In our study, we used the model of *Ledieu et al.* [1986] to relate θ to ε_r, namely,

$$\varepsilon_r = \left(\frac{\theta - c}{d}\right)^2 \tag{6}$$

where we fixed $c = -0.1933$ and $d = 0.1264$ for the three textural classes [*Lambot et al.*, 2004b], given the relatively small variation of these parameters for a wide range of soils. Topp's model [*Topp et al.*, 1980] is also used for analyzing the stability of the inverse solution with respect to petrophysical modeling errors.

[13] The model of *Rhoades et al.* [1976] was used to relate soil water content to electric conductivity, as

$$\sigma = \left(a\theta^2 + b\theta\right)\sigma_w + \sigma_s \tag{7}$$

where a and b are soil specific parameters (defined in Table 1 for the three soils), σ_w is the electric conductivity of the soil water (we fixed it to $\sigma_w = 0.075$ S m^{-1}), and σ_s is the electric conductivity of the dry soil (defined in Table 1 for the three soils).

2.5. Objective Function and Optimization

[14] The inverse problem is formulated by the least squares criterion in terms of electromagnetic data and the objective function to minimize is accordingly defined as follows:

$$\phi(\mathbf{b}) = \sum_t \sum_f \left| G_{xx}^{\uparrow *}(f,t) - G_{xx}^{\uparrow}(f,t,\mathbf{b}) \right|^2 \tag{8}$$

where $G_{xx}^{\uparrow}{}^*(f,t)$ and $G_{xx}^{\uparrow}(f,t,\mathbf{b})$ are, respectively, the measured and modeled complex Green's functions, and $\mathbf{b} = [\alpha, n, K_s]$ is the parameter vector to be estimated. Since the Green's function is a complex quantity, the difference between observed and modeled data is expressed by the amplitude of the differences in the complex plane. As the objective function is nonlinear and may be characterized by multiple local minima, it is minimized using a global approach based on the global multilevel coordinate search algorithm (GMCS) [*Huyer and Neumaier*, 1999] that we combined sequentially with the classical Nelder-Mead simplex (NMS) [*Lagarias et al.*, 1998] for improved efficiency and robustness. We observed that local optimization strategies alone usually fail to solve the proposed inverse problem (results not presented).

3. Numerical Experiments

3.1. Hydrodynamic Events and Time-Lapse GPR Data

[15] Numerical experiments have been performed to investigate the well posedness of the proposed integrated hydrogeophysical inversion procedure for different textured soils and different hydrodynamic boundary conditions. We simulated transient infiltration events in coarse, medium and fine soils, as defined in the European database HYPRES [*Wösten et al.*, 1999]. The corresponding hydraulic properties, following MVG model, are depicted in Table 1. Realistic values for the petrophysical parameters of the Rhoades' model are also provided for the three considered soils [*Rhoades et al.*, 1990].

[16] Equation (1) was solved numerically using the finite difference WAVE model [*Vanclooster et al.*, 1996] for 1-D flow simulation. The vertical flow domain extended from the soil surface to a depth of $L = 0.3$ m, thereby representing the most sensitive zone for the GPR measurements. The profile was discretized into 60 equidistant linear elements, representing each $dz = 0.005$ m. Such fine discretization was required to represent continuously varying profiles in the electromagnetic model. Namely, layer thicknesses should be less than one tenth the minimal wavelength $\lambda_{\min}$, in our case:

$$dz \leq \frac{\lambda_{\min}}{10} = \frac{\frac{c_0}{\sqrt{\varepsilon_{r,\max}}}}{10 f_{\max}} = 0.003 \text{ m} \simeq 0.005 \text{ m} \tag{9}$$

with $f_{\max} = 2000$ MHz and $\varepsilon_{r,\max} = 31.8$, corresponding to the maximum water content $\theta_{\max} = 0.52$ (see Table 1).

[17] Table 2 sketches the twelve inversion cases that were considered in this study: 4 scenarios × 3 soil types. For each coarse, medium and fine texture of soil we first considered three constant relative flux values for the top boundary condition (see equation (2b)), namely, $q(t) = q =$

Table 2. Convergence of the Hydrogeophysical Inversion Toward the Actual Soil Hydraulic Parameters for the Different Textured Soils and Scenarios

	Flux q (cm/min)	t_{max} (min)	Convergence
	Coarse (K_s = 0.0417 cm/min)		
Scenario 1	K_s/5	1000	yes
Scenario 2	K_s/20	3400	yes
Scenario 3	K_s/50	7500	yes
Scenario 4	$q(t)$	60000	yes
	Medium (K_s = 0.0084 cm/min)		
Scenario 1	K_s/5	4500	yes
Scenario 2	K_s/20	15000	yes
Scenario 3	K_s/50	29500	yes
Scenario 4	$q(t)$	100000	yes
	Fine (K_s = 0.0172 cm/min)		
Scenario 1	K_s/5	2200	no
Scenario 2	K_s/20	8500	yes
Scenario 3	K_s/50	18000	yes[a]
Scenario 4	$q(t)$	100000	yes

[a]Insignificant error in convergence.

[K_s/5, K_s/20, K_s/50], referred to as scenarios 1, 2, and 3, respectively. The initial condition for these scenarios was expressed in terms of pressure head considering hydrostatic equilibrium (see equation (2b)) with $h_i(L) = -10^5$ cm, thereby representing dry conditions. Exploring a wide range of water contents is necessary to ensure uniqueness in soil hydrodynamic inverse problems [*Kool and Parker*, 1988]. We considered 25 observation times for the GPR measurements, with logarithmically increasing time steps. These were set in order to observe not only varying infiltration fronts with depth but also varying surface water content (water content at the interface between the soil and the atmosphere), to which the radar measurements will be particularly sensitive.

[18] Figure 2 illustrates infiltration events for the three textured soils and assuming different relative constant values for q, resulting in contrasted water content profile shapes and different GPR responses. The presented profiles correspond to the observation times. The maximal observation time corresponds to the arrival of the infiltration front at the bottom of the considered spatial domain. We can observe that the high flux in the coarse soil leads to step-like profiles. For the two other soils, the profiles are more gradual, which may be critical to wave reflections [*Lambot et al.*, 2004b; *Bano*, 2006]. It is worth noting that the water content variation range decreases for finer soils. However, absolute volumetric water content variations are always larger than 25%. This is a requisite to provide enough information to estimate uniquely the unsaturated soil hydraulic properties using inverse modeling [e.g., *Kool and Parker*, 1988].

[19] The time-lapse Green's functions corresponding to the three scenarios presented in Figure 2 are depicted in Figure 3. Similar results were obtained for the other constant flux scenarios (1–3). Data are presented not only in the frequency domain, in terms of amplitude and phase of the Green's function, but also in the time domain for substantiating interpretation. We considered the radar data to be acquired over the ultrawide-frequency range 200–2000 MHz. A constant frequency step of 20 MHz was used for the inversions, resulting in 91 observation frequencies.

[20] Initially, we observe that in all cases, the infiltration events have an effect on the time-lapse Green's function. This means that the proximal radar data contain some information on the soil hydraulic properties. From the time

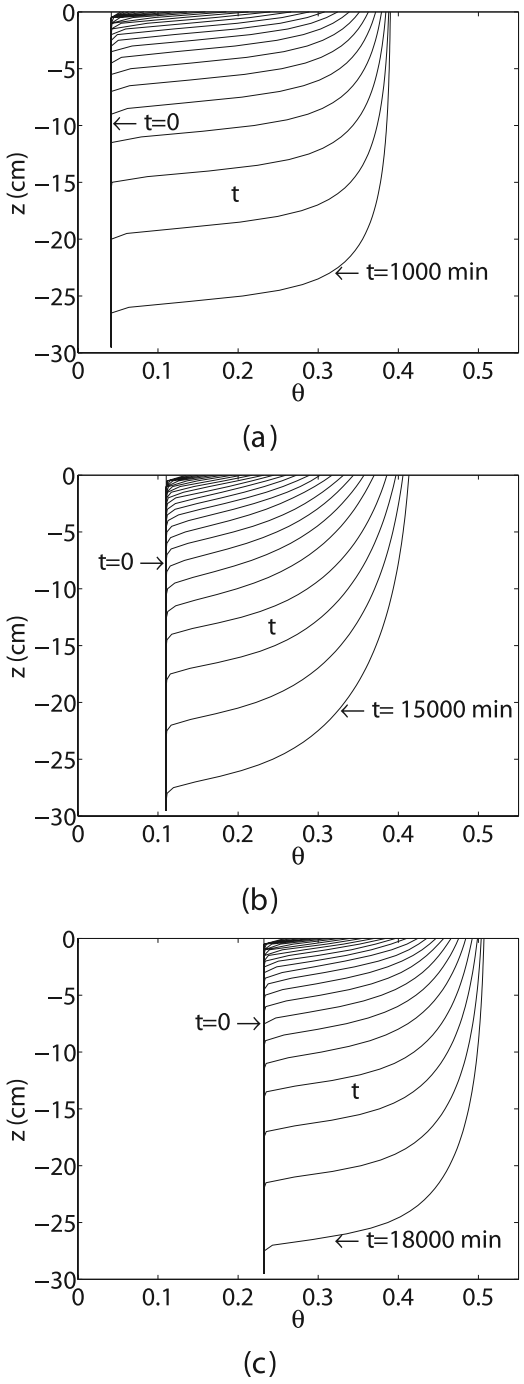

Figure 2. Time-dependent water content profiles for the three textured soils and different relative fluxes q for the top boundary condition: (a) coarse with $q = K_s/5$ (scenario 1), (b) medium with $q = K_s/20$ (scenario 2), and (c) fine with $q = K_s/50$ (scenario 3). Variable z is depth, θ is volumetric water content, and t is time. Time steps for observation times are logarithmically increasing.

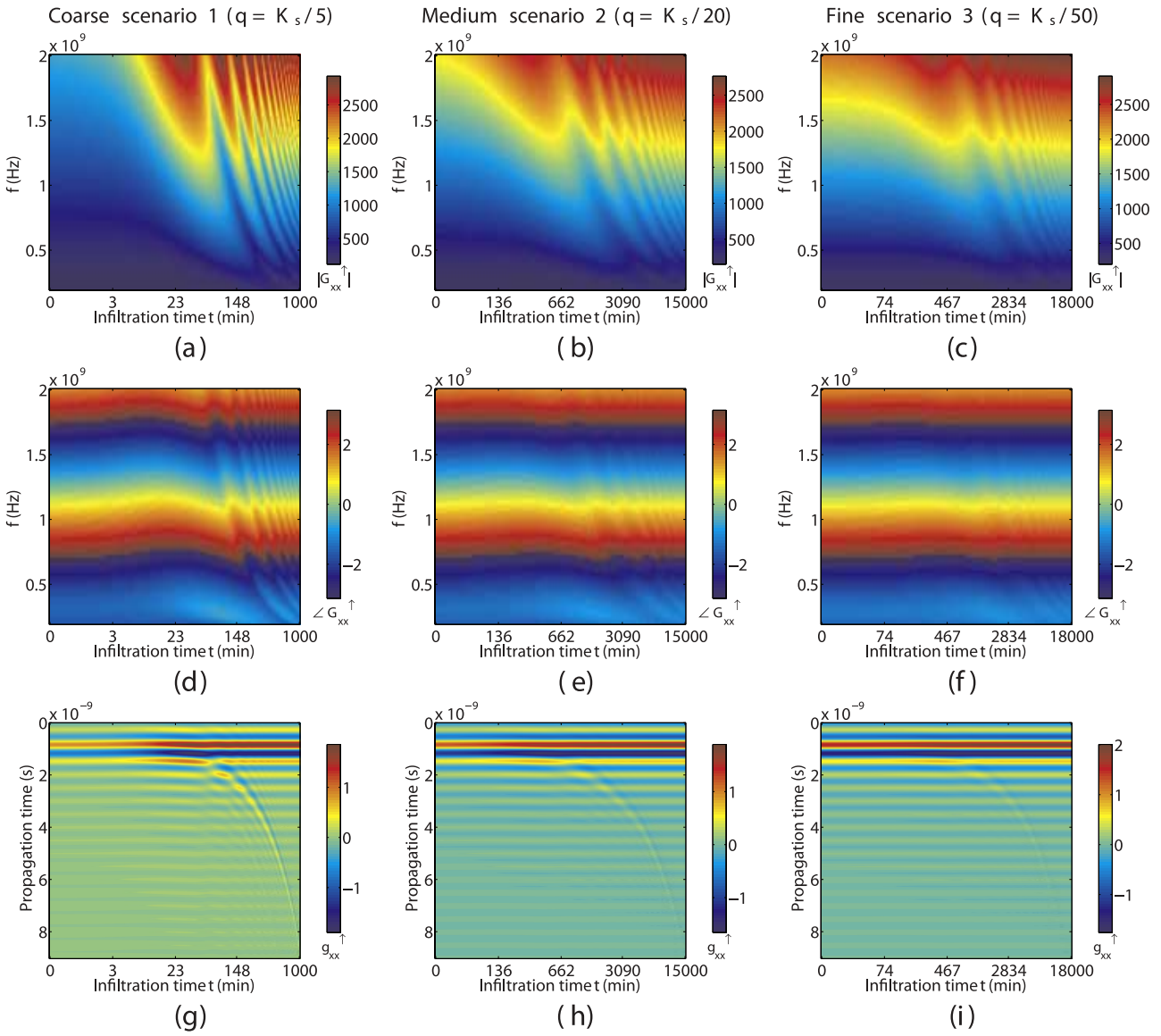

Figure 3. Time-lapse Green's function in both the frequency domain ($|G_{xx}^{\uparrow}|$ denotes amplitude and $\angle G_{xx}^{\uparrow}$ denotes phase of the Green's function) and time domain for the coarse, medium, and fine soils (f is frequency). Time steps for infiltration time are logarithmically increasing.

domain data, we see that these variations mainly originate from both the surface and infiltration front reflections. Naturally, all other electromagnetic phenomena are also taken into account in the inversion process, such as distortion effects. For the lower frequencies, time-lapse variations are negligible. This originates from the poor range resolution (large wavelength) at these frequencies compared to the spatial flow domain. The finer the soil, the weaker is the GPR response to infiltration. This is to be attributed to two factors. First, as mentioned above, more gradual profiles are less advantageous to radar reflections. Second, finer soils, especially containing clay, will typically have a higher electric conductivity and lead to more significant GPR wave attenuation. This effect is particularly apparent in the time domain Green's function for the fine soil (see Figure 3), for which the infiltration front reflection is quite weak. It is worth noting that the oscillating patterns in the time domain plots are artifacts of the inverse Fourier transformation of data taken over a limited frequency range (200–2000 MHz).

[21] In order to represent more realistic conditions, we considered an additional scenario, referred to as scenario 4, with time-variable flux $q(t)$, including real precipitation and evaporation data from a meteorological station in central Belgium (see Figure 4). The bottom boundary condition was set up as free drainage. In practical applications, the depth-dependent initial conditions (at time $t = t_i$) in the hydrodynamic model are poorly known or not known at all. In this scenario, we therefore assumed these initial conditions to be a priori unknown. These were estimated from arbitrary initial conditions (at time $t = t_i' < t_i$) using the hydrodynamic model subject to the time-variable boundary conditions for a sufficiently long time ($t_i - t_i'$) so that the pressure head (or water content) profile at $t = t_i$ is independent of the arbitrary profile at $t = t_i'$. This concept is

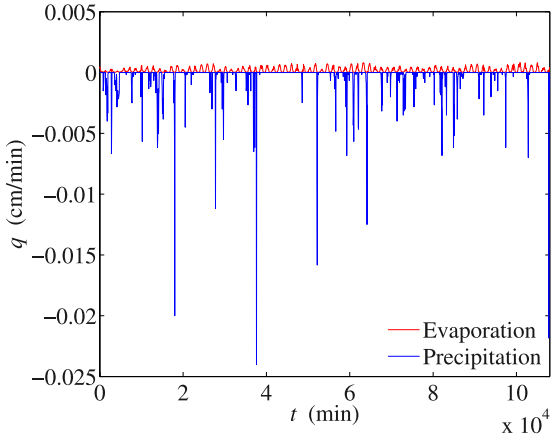

Figure 4. Real precipitation and evaporation flux values (q, negative for downward flux) as a function of time t recorded over a 2.5-month period (meteorological station in Belgium) for scenario 4. Observation time step is 60 min.

illustrated in Figure 5 for the three textured soils. Water content at depth $z = 0.25$ m was simulated as a function of time assuming four different initial pressure heads at $t = t_i'$, namely, $h_i'(L) = [-10^1, -10^2, -10^3, -10^4]$ cm. We clearly observe that all water content time series tend to the same values after some time. Time of convergence (corresponding to t_i as defined above) is smaller for lower depths and larger for higher depths. It depends on the soil type and also on the top boundary conditions. In particular, artificial top boundary conditions can be set up to have earlier convergence (results not presented). The shaded areas in Figure 5 represent the time range for which the time-lapse GPR data were acquired, with 100 evenly spaced observation times. Maximum simulation times for the hydrodynamic events were set up to $t_{max} = 6 \times 10^4$ min for coarse and $t_{max} = 10^5$ min for medium- and fine-textured soils. The synthetic GPR data sets were generated assuming $h_i'(L) = -10^5$ cm, while inversions were performed assuming $h_i'(L) = -10^2$ cm. This represents a relatively large difference or initial condition error. Figure 6 represents the amplitude of the time-lapse Green's function for medium soil subject to the time-variable boundary conditions. As for previous scenarios (1–3), the time-lapse variations indicate that the radar measurements are well influenced by the hydrodynamic events.

3.2. Uniqueness Analysis

[22] To analyze the uniqueness of the inverse solution in the proposed integrated method, we have inverted the frequency domain, time-lapse synthetic Green's functions for the twelve scenarios (4 scenarios × 3 soil types) described above. The benefit of this numerical approach is that the true soil hydraulic properties are known and that the time-lapse data are perfectly described by the integrated

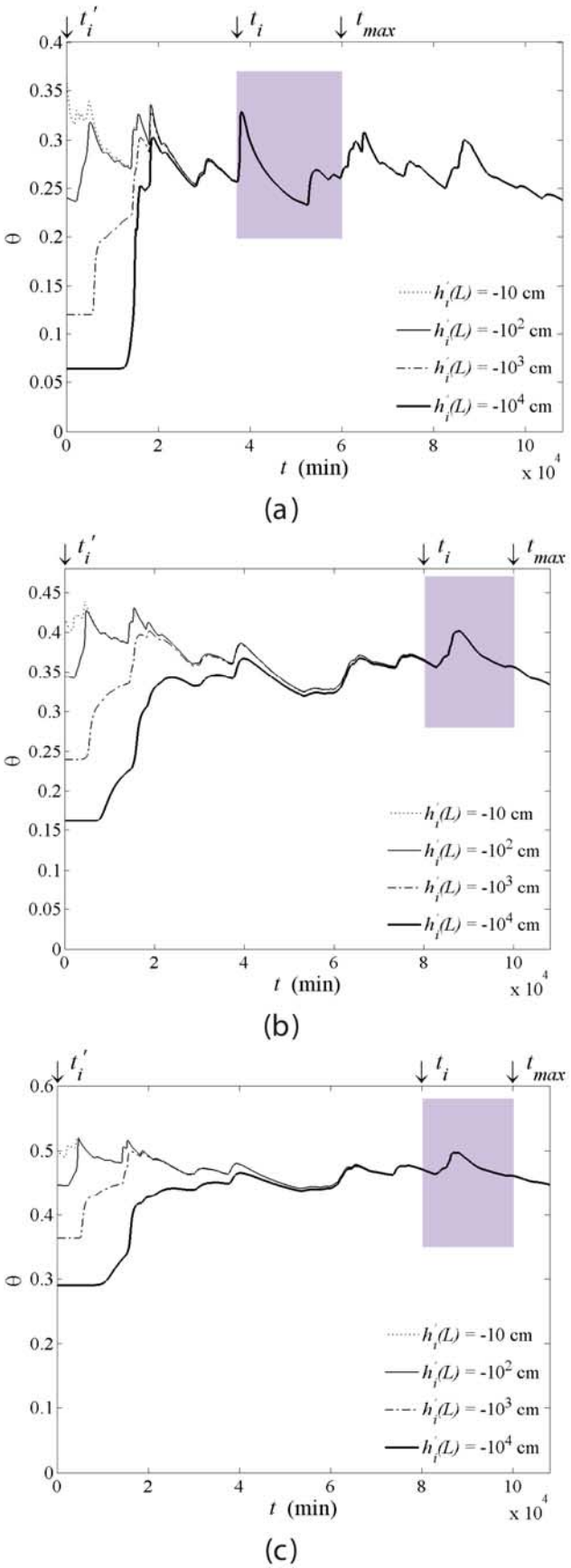

Figure 5. Water content time series for depth $z = 25$ cm for the three textured soils (a) coarse, (b) medium, and (c) fine assuming different initial condition h_i' and variable fluxes $q(t)$ (scenario 4) over a 2.5-month period. Shaded areas represent radar measurement periods with 100 evenly spaced observation times.

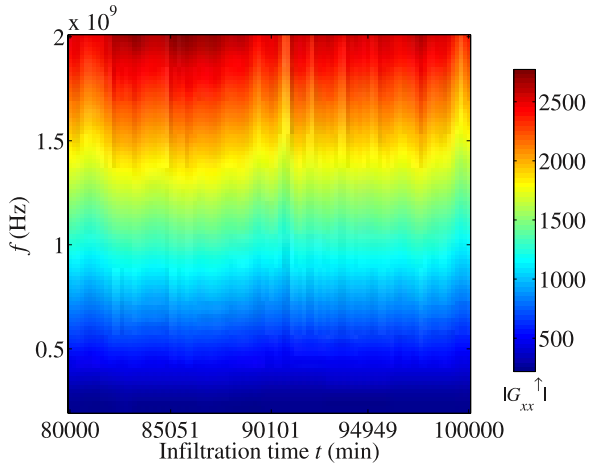

Figure 6. Time-lapse Green's function amplitude in the frequency domain for medium soil subject to time-variable boundary conditions (scenario 4).

hydrodynamic-petrophysical-electromagnetic model, i.e., without measurement and modeling errors. For all inversions, the optimization parameter space was identical and set relatively large so that it contained simultaneously all the parameter vectors corresponding to the three textured soils defined in HYPRES and also matched prevailing environmental conditions, namely, $0.010 \leq \alpha \leq 0.050$ cm^{-1}; $1.05 \leq n \leq 2.00$; $10^{-3} \leq K_s \leq 10^{-1}$ cm min^{-1}. However, it is worth noting that K_s may vary of several orders of magnitude within a single soil type.

[23] Table 2 shows the convergence of the inverse estimates toward the true solution. For coarse and medium soil scenarios, all three parameters α, n, and K_s were exactly retrieved after about 1350–1500 iterations. This demonstrates that, theoretically, there is enough information in the time-lapse, off-ground GPR data to estimate these key soil hydraulic parameters. For the fine soil, less satisfactory results were obtained and the true solution was retrieved exactly in only two scenarios (2 and 4). For the two other scenarios (1 and 3), either the solution was approximate or relatively far from the true parameters. Enhancing the parameterization of the optimization algorithm, e.g., by significantly increasing the maximum number of iterations (up to 20,000), did not improve the results. It is worth mentioning that for scenario 4, the solution was exactly retrieved for all soil types, notwithstanding the unknown initial conditions. These results suggest that pressure head information may not be especially required for identifying the unsaturated soil hydraulic properties and that time-variable boundary conditions may provide more information regarding soil hydraulic properties compared to constant fluxes. The computation time for scenarios 1–3 was about 4–8 hours using 16 parallel processors of the JUMP supercomputer (Forschungszentrum Jülich, Germany). Scenarios 4 needed about 10 times more computing resources given the longer hydrodynamic simulations (not parallelized code) and the larger number of observation times for the GPR Green's function computation. In order to provide further insights on the uniqueness of the inverse solution and elucidate the nonconvergence cases, we have computed the objective functions with respect to the three parameter pairs α-n, n-K_s, and α-K_s for the cases shown in Figures 2 and 3, namely, coarse soil with scenario 1, medium soil with scenario 2, and fine soil with scenario 3. The range of each parameter has been divided into 50 discrete values, resulting in 2500 objective function calculations for each contour plot. The objective function response surfaces are presented in Figure 7. The white star marker represents the true values of the parameters, while the red triangle corresponds to the solution found by the GMCS-NMS optimization algorithm. The white areas correspond to parameter sets for which the numerical hydrodynamic model did not converge. As expected from the optimization results, the global minimum is well defined for the coarse and medium soils. For the fine soil, the minimum region in the α-n and n-K_s parameter planes is relatively flat, following α and K_s directions, respectively. In these two parameter planes, α and K_s are not correlated to parameter n but show a poor sensitivity which resulted in nonconvergence of the optimization algorithm toward the true solution. The origin of this insensitivity is twofold. First, as emphasized above, the high electric conductivity of the fine soil strongly attenuates GPR wave reflections, thereby decreasing information content in the time-lapse Green's function. A high electric conductivity also contributes to strengthen the surface reflection, which simultaneously decreases GPR wave penetration into the soil. A high electric conductivity also lessens sensitivity of the surface reflection with respect to surface dielectric permittivity and correlated water content [*Lambot et al.*, 2006b]. Second, the more gradual electromagnetic profiles for the fine soil amplify these unfavorable effects. We observed using additional simulations that reducing electric conductivity for the fine soil enables proper convergence toward the true solution. The flux value controlling profile shapes does not appear to be the most important factor determining the uniqueness of the inverse solution. For parameter plane α-K_s, we observe for the three soils a positive correlation between parameters α and K_s. As measurement and modeling errors typically further flatten the objective function topography, such correlation may lead to instability of the inverse solution (see stability analysis below). Finally, it is worth noting that the topography of the objective function in these 2-D plots does not contain any oscillations nor local minima, which is favorable for fast and robust optimization. The topography is however expected to be more complex in higher dimensions (three or more parameters to optimize) and the use of local optimization was not sufficient to ensure proper optimization for the scenarios analyzed in this study (results not shown).

3.3. Stability Analysis

[24] In addition to the uniqueness of the inverse solution, we have analyzed its stability with respect to errors in the fixed hydraulic parameters (θ_r, θ_s, l), petrophysical parameters (a, b, σ_s) and model (Ledieu vs. Topp), initial conditions ($h_i(z)$) in case they are assumed to be known, and top boundary condition ($q(t)$). The analysis has been conducted only for three scenarios, corresponding to Figure 2, namely, coarse with $q = K_s/5$ (scenario 1), medium with $q = K_s/20$ (scenario 2), and fine with $q = K_s/50$ (scenario 3). Inversions have been performed considering relative errors of 1% and 10% in the parameters, respectively. Additionally, we have considered particular cases in

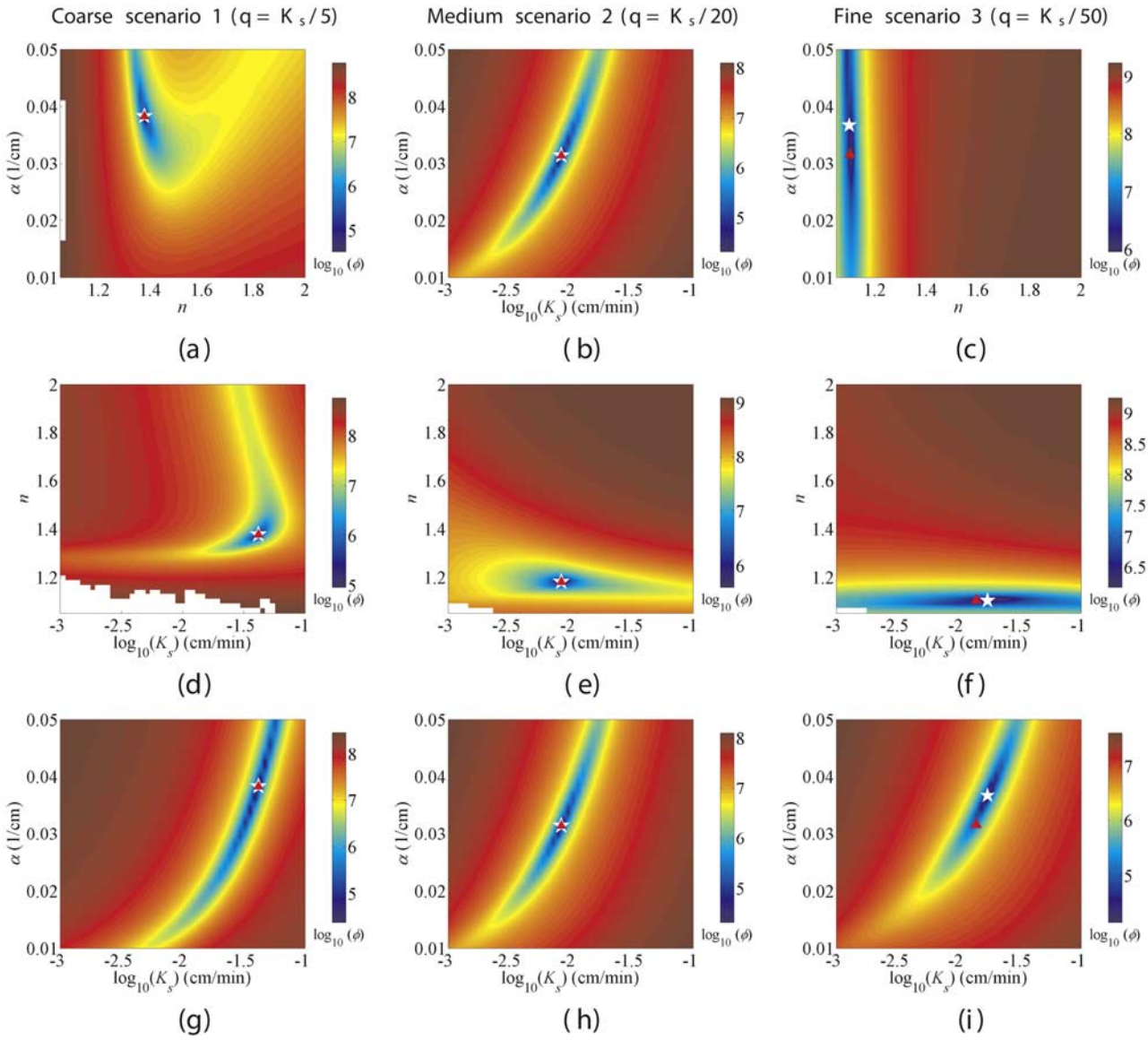

Figure 7. Response surfaces of the objective function logarithm $\log_{10}(\phi)$ in the α-n, n-K_s, and α-K_s parameter planes. The white star markers represent the true parameter values. The red triangle markers represent the parameter values obtained by inversion. The white areas correspond to parameter sets for which the hydrodynamic model does not converge.

the MVG model, where θ_r is fixed to 0 [*Fuentes et al.*, 1992; *van Dam et al.*, 1994] and l is fixed to 0.5 [*van Genuchten*, 1980], as commonly used parameterizations. Inversion results are presented in Table 3. Figure 8 depicts the corresponding water retention curves, compared to the true ones, for the less favorable scenarios of the stability analysis.

[25] Relative errors of 1% in the fixed parameters always led to negligible errors in the inversely estimated parameters. For 10% relative errors in the petrophysical parameters of the Rhoades' model, similar results were obtained, which is particularly advantageous for practical applications as these parameters are not easily accessible and are expected to vary within a field. The inverse estimates are also not very sensitive to 10% relative errors in l, θ_r, and initial pressure head profile. For this last case, it is worth noting that such low sensitivity to the initial pressure head may be due to the very dry conditions and less satisfactory results may be obtained in wet conditions. Fixing $\theta_r = 0$ leads to significant errors only for the coarse soil (see Figure 8a). This is to be attributed to the larger difference compared to the true residual water content for that soil ($\theta_r = 0.025$). For instance, *Vereecken et al.* [1989] observed experimentally that fixing θ_r to 0 results in a loss of flexibility in describing the water retention characteristics. For $l = 0.5$, more substantial errors were obtained. However, as can be seen in Figure 8c, the results are still accurate enough to clearly differentiate the three different textured soils. For precise estimation of the hydraulic conductivity function, fixing l to a unique value for different soils should be avoided [*Vereecken*, 1995]. Errors of 10% in θ_s lead to direct errors in the water retention curve for the lower-

Table 3. Inversely Estimated Parameters for the Three Textured Soils Considering Different Errors on the Fixed Hydraulic and Petrophysical Parameters[a]

	Coarse With Scenario 1			Medium With Scenario 2			Fine With Scenario 3		
	α	n	$\log_{10}(K_s)$	α	n	$\log_{10}(K_s)$	α	n	$\log_{10}(K_s)$
True values	0.0383	1.3774	−1.3779	0.0314	1.1804	−2.0757	0.0367	1.1012	−1.7645
				Error on θ_r					
$\theta_r^* = 1.01\ \theta_r$	0.0384	1.3790	−1.3811	0.0314	1.1805	−2.0762	0.0367	1.1012	−1.7645
$\theta_r^* = 1.10\ \theta_r$	0.0380	1.3967	−1.4130	0.0314	1.1814	−2.0821	0.0319	1.1032	−1.8517
$\theta_r^* = 0$	0.033	1.2793	−1.2438	0.0280	1.1738	−2.0814	0.0317	1.0999	−1.8210
				Error on θ_s					
$\theta_s^* = 1.01\ \theta_s$	0.0447	1.3718	−1.2705	0.0334	1.1802	−2.0212	0.0433	1.1005	−1.6334
$\theta_s^* = 1.10\ \theta_s$	0.0989	1.3499	−0.6101	0.0534	1.1805	−1.6113	0.0528	1.1080	−1.2709
				Error on l					
$l^* = 1.01\ l$	0.0378	1.3780	−1.3840	0.0315	1.1803	−2.0792	0.0391	1.1004	−1.7281
$l^* = 1.10\ l$	0.0336	1.3832	−1.4220	0.0437	1.1733	−1.9259	0.0366	1.1012	−1.7895
$l^* = 0.5$	0.0744	1.3498	−1.1939	0.0099	1.2097	−2.1005	0.0091	1.1217	−2.2972
				Error on a					
$a^* = 1.01\ a$	0.0384	1.3773	−1.3785	0.0314	1.1804	−2.0756	0.0206	1.1086	−2.1245
$a^* = 1.10\ a$	0.0394	1.3764	−1.3661	0.0314	1.1804	−2.0761	0.0325	1.1027	−1.8356
				Error on b					
$b^* = 1.01\ b$	0.0383	1.3774	−1.3798	0.0314	1.1804	−2.0756	0.0279	1.1047	−1.9342
$b^* = 1.10\ b$	0.0384	1.3773	−1.3789	0.0314	1.1804	−2.0757	0.0279	1.1047	−1.9343
				Error on σ_s					
$\sigma_s^* = 1.01\ \sigma_s$	0.0383	1.3774	−1.3799	0.0314	1.1804	−2.0756	0.0208	1.1086	−2.1114
$\sigma_s^* = 1.10\ \sigma_s$	0.0383	1.3774	−1.3797	0.0314	1.1804	−2.0756	0.0329	1.1025	−1.8315
				Error on q					
$q^* = 1.01\ q$	0.0262	1.4051	−1.6205	0.0288	1.1838	−2.1483	0.0294	1.1048	−1.9123
$q^* = 1.10\ q$	0.0389	1.7511	−2.0437	0.0168	1.2111	−2.6338	0.0160	1.1197	−2.4238
				Error on Initial Pressure Head Profile $h_i(z)$					
$h_i^*(z) = 1.01\ h_i(z)$	0.0383	1.3770	−1.3792	0.0311	1.1804	−2.0796	0.0320	1.1027	−1.8450
$h_i^*(z) = 1.10\ h_i(z)$	0.0382	1.3732	−1.3724	0.0286	1.1803	−2.1150	0.0294	1.1027	−1.8791

[a]The superscript asterisk denotes parameters with an error.

pressure heads, but these errors progressively decrease at higher-pressure heads (see Figure 8b). Indeed, the saturated water content θ_s directly determines water content at zero pressure head in the water retention curve, so an error on θ_s directly results in an error on that part of the water retention curve. Relative errors of 10% in the flux caused significant errors in the estimated parameters for the coarse soil scenario 1 only, which is partly due to the relatively high flux ($q = K_s/5$) as compared to the two other scenarios 2 and 3 (see Figure 8d).

[26] In addition, to represent a more realistic case where all errors are present, we simultaneously considered a relative error of 10% in all the fixed parameters. The inversion results, presented in Figure 9, showed substantial errors for the estimation of the hydraulic properties in low-pressure heads, which originates mainly from the direct effect of the error on θ_s. For higher-pressure heads, the obtained water retention curves tend to the true ones, except for the coarse soil. This is to be attributed to the higher flux and corresponding relative error considered for that soil (see Figure 8d).

[27] Finally, we investigated for scenario 4 the effect of an error in the petrophysical model relating dielectric permittivity to water content. Namely, synthetic GPR data were generated using the model of Ledieu while inversions were carried out assuming Topp's relationship. Results are presented in Figure 10. Satisfactory results were obtained for coarse and medium soils, while more significant errors were obtained for fine soil.

4. Conclusions

[28] Numerical experiments were performed to analyze the well posedness of the proposed hydrogeophysical inverse problem for time-lapse proximal GPR. The uniqueness analysis demonstrated that provided that the soil electric conductivity is not too high, which mainly applies to coarse- and medium-textured soils, enough information is contained in the time-lapse radar data to uniquely estimate three key soil hydraulic parameters, namely, α, n, and K_s of the MVG model. A low hydraulic conductivity such as usually encountered for fine soils is disadvantageous to uniqueness as it may lead to vertical water content profiles with relatively gradual changes, which precludes radar reflections. The stability analysis showed that possible errors on other model parameters (i.e., fixed in the inversion) generally do not lead to significant errors in the

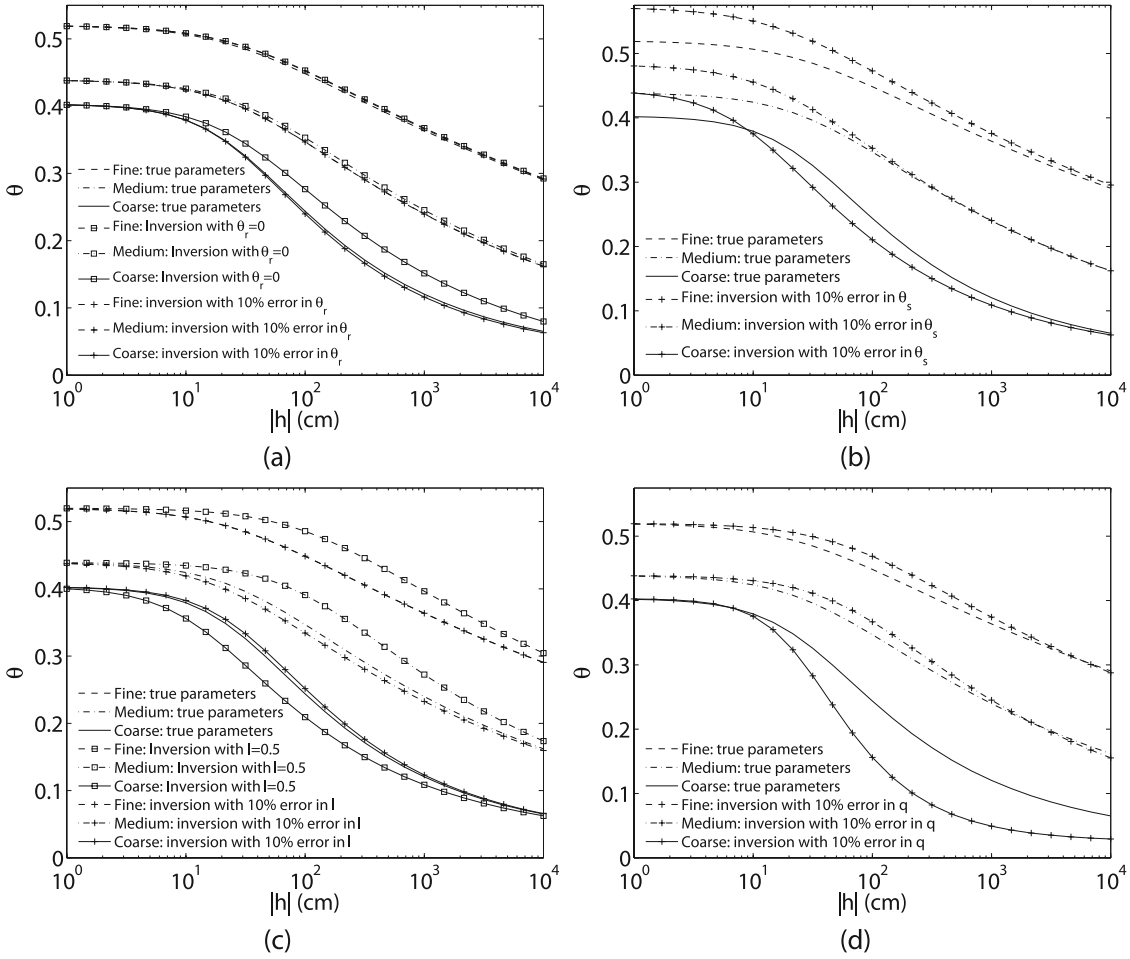

Figure 8. Actual and inversely estimated water retention curves for the three textured soils assuming independent errors on (a) θ_r, (b) θ_s, (c) l, and (d) q. Actual relative flux values are $q = K_s/5$ (scenario 1) for coarse, $q = K_s/20$ (scenario 2) for medium, and $q = K_s/50$ (scenario 3) for fine.

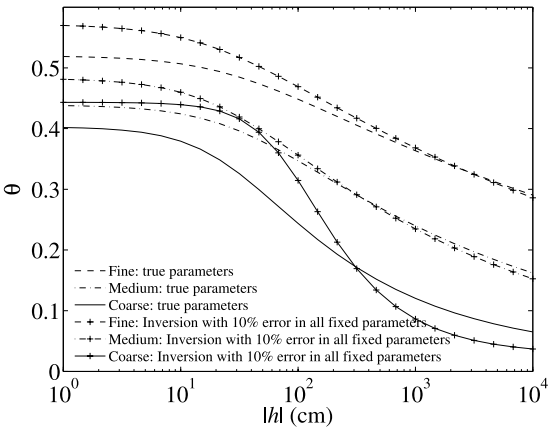

Figure 9. Actual and inversely estimated water retention curves for the three textured soils assuming simultaneous 10% errors on all fixed parameters, namely, θ_r, θ_s, l, q, a, b, and σ_s. Actual relative flux values are $q = K_s/5$ (scenario 1) for coarse, $q = K_s/20$ (scenario 2) for medium, and $q = K_s/50$ (scenario 3) for fine.

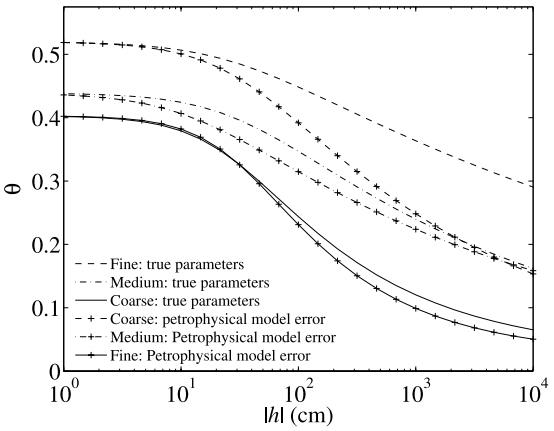

Figure 10. Actual and inversely estimated water retention curves for the three textured soils using Ledieu's model to generate the GPR data and Topp's model to retrieve the unknown parameters (scenario 4).

estimated water retention and hydraulic conductivity parameters. However, we recommend to pay particular attention to an accurate estimation of the saturated water content θ_s and top flux q (for infiltration) for which stability is less advantageous. In practical applications, θ_r and θ_s can be directly retrieved from the GPR data themselves in dry and saturated soil conditions, respectively, or using pedotransfer functions. When applied at the field scale in a mapping context, the proposed procedure has the theoretical potential of remotely providing estimates of both the horizontal distribution of the shallow soil hydraulic properties and 3-D images of soil water content with a high spatial resolution. Future research will focus on the application of the method in real laboratory and field conditions. The proposed approach appears to be particularly promising for mapping the shallow soil hydraulic properties at the field scale with a high spatial resolution. We however emphasize that the presented results are theoretical and that additional limitations are expected in the field, such as larger errors in some fixed parameters, 3-D flow phenomena, preferential flows, or local heterogeneities (at the GPR measurement scale), which have not been taken into account in the present analysis.

[29] **Acknowledgments.** This work was supported by the Forschungszentrum Jülich GmbH (Germany), Fonds National de la Recherche Scientifique (FNRS) and Université Catholique de Louvain (Belgium), and Delft University of Technology (Netherlands). The authors are grateful to Marc Grasmueck, Niklas Linde, an anonymous reviewer, and Fred Day-Lewis for their constructive comments for improving the manuscript.

References

Annan, A. P. (2005), GPR methods for hydrogeological studies, in *Hydrogeophysics*, *Water Sci. Technol. Libr. Ser.*, vol. 50, edited by Y. Rubin and S. Hubbard, pp. 185–213, Springer, New York.

Bano, M. (2006), Effects of the transition zone above a water table on the reflection of GPR waves, *Geophys. Res. Lett.*, *33*, L13309, doi:10.1029/2006GL026158.

Behaegel, M., P. Sailhac, and G. Marquis (2007), On the use of surface and ground temperature data to recover soil water content information, *J. Appl. Geophys.*, *62*(3), 234–243.

Binley, A., G. Cassiani, R. Middleton, and P. Winship (2002), Vadose zone flow model parameterisation using cross-borehole radar and resistivity imaging, *J. Hydrol.*, *267*, 147–159.

Blumberg, D. G., V. Freilikher, I. V. Lyalko, L. D. Vulfson, A. L. Kotlyar, V. N. Shevchenko, and A. D. Ryabokonenko (2000), Soil moisture (water-content) assessment by an airborne scatterometer: The Chernobyl disaster area and the Negev Desert, *Remote Sens. Environ.*, *71*(3), 309–319.

Born, M., and E. Wolf (1980), *Principles of Optics*, 6th ed., Pergamon, Oxford, U. K.

Brocca, L., R. Morbidelli, F. Melone, and T. Moramarco (2007), Soil moisture spatial variability in experimental areas of central Italy, *J. Hydrol.*, *333*, 356–373.

Cassiani, G., and A. Binley (2005), Modeling unsaturated flow in a layered formation under quasi-steady state conditions using geophysical data constraints, *Adv. Water Resour.*, *28*(5), 467–477.

Dirksen, C., and S. Dasberg (1993), Improved calibration of time-domain reflectometry soil-water content measurements, *Soil Sci. Soc. Am. J.*, *57*, 660–667.

Ersahin, S., and A. R. Brohi (2006), Spatial variation of soil water content in topsoil and subsoil of a typic ustifluvent, *Agric. Water Manage.*, *83*(1–2), 79–86.

Fuentes, C., R. Haverkamp, and J. Y. Parlange (1992), Parameter constraints on closed-form soil water relationships, *J. Hydrol.*, *134*, 117–142.

Galagedara, L. W., G. W. Parkin, J. D. Redman, P. von Bertoldi, and A. L. Endres (2005), Field studies of the GPR ground wave method for estimating soil water content during irrigation and drainage, *J. Hydrol.*, *301*, 182–197.

Heimovaara, T. J. (1994), Frequency domain analysis of time domain reflectometry waveforms: 1. Measurement of the complex dielectric permittivity of soils, *Water Resour. Res.*, *30*, 189–199.

Heimovaara, T. J., J. A. Huisman, J. A. Vrugt, and W. Bouten (2004), Obtaining the spatial distribution of water content along a TDR probe using the SCEM-UA Bayesian inverse modeling scheme, *Vadose Zone J.*, *3*, 1128–1145.

Hubbard, S., J. Chen, K. Williams, J. Peterson, and Y. Rubin (2005), Environmental and agricultural applications of GPR, in *Proceedings of the 3rd International Workshop on Advanced Ground Penetrating Radar*, edited by A. Gorriti and S. Lambot, pp. 45–49, Delft Univ. of Technol., Delft, Netherlands.

Huisman, J. A., S. S. Hubbard, J. D. Redman, and A. P. Annan (2003), Measuring soil water content with ground penetrating radar: A review, *Vadose Zone J.*, *2*, 476–491.

Hupet, F., and M. Vanclooster (2002), Intraseasonal dynamics of soil moisture variability within a small agricultural maize cropped field, *J. Hydrol.*, *261*, 86–101.

Huyer, W., and A. Neumaier (1999), Global optimization by multilevel coordinate search, *J. Global Optim.*, *14*(4), 331–355.

Johnson, R. H., and E. P. Poeter (2007), Insights into the use of time-lapse GPR data as observations for inverse multiphase flow simulations of DNAPL migration, *J. Contam. Hydrol.*, *89*(1–2), 136–155.

Jury, W. A., W. R. Gardner, and W. H. Gardner (1996), *Soil Physics*, 5th ed., John Wiley, New York.

Kelleners, T. J., D. A. Robinson, P. J. Shouse, J. E. Ayars, and T. H. Skaggs (2005), Frequency dependence of the complex permittivity and its impact on dielectric sensor calibration in soils, *Soil Sci. Soc. Am. J.*, *69*, 67–76.

Kool, J. B., and J. C. Parker (1988), Analysis of the inverse problem for transient unsaturated flow, *Water Resour. Res.*, *24*, 817–830.

Kool, J. B., J. C. Parker, and M. T. van Genuchten (1985), Determining soil hydraulic properties from one-step outflow experiments by parameter estimation: Theory and numerical studies, *Soil Sci. Soc. Am. J.*, *49*, 1348–1354.

Kowalsky, M. B., S. Finsterle, J. Peterson, S. Hubbard, Y. Rubin, E. Majer, A. Ward, and G. Gee (2005), Estimation of field-scale soil hydraulic and dielectric parameters through joint inversion of GPR and hydrological data, *Water Resour. Res.*, *41*, W11425, doi:10.1029/2005WR004237.

Lagarias, J. C., J. A. Reeds, M. H. Wright, and P. E. Wright (1998), Convergence properties of the Nelder-Mead simplex method in low dimensions, *SIAM J. Optim.*, *9*(1), 112–147.

Lambot, S., M. Javaux, F. Hupet, and M. Vanclooster (2002), A global multilevel coordinate search procedure for estimating the unsaturated soil hydraulic properties, *Water Resour. Res.*, *38*(11), 1224, doi:10.1029/2001WR001224.

Lambot, S., F. Hupet, M. Javaux, and M. Vanclooster (2004a), Laboratory evaluation of a hydrodynamic inverse modeling method based on water content data, *Water Resour. Res.*, *40*, W03506, doi:10.1029/2003WR002641.

Lambot, S., J. Rhebergen, I. van den Bosch, E. C. Slob, and M. Vanclooster (2004b), Measuring the soil water content profile of a sandy soil with an off-ground monostatic ground penetrating radar, *Vadose Zone J.*, *3*, 1063–1071.

Lambot, S., E. C. Slob, I. van den Bosch, B. Stockbroeckx, and M. Vanclooster (2004c), Modeling of ground-penetrating radar for accurate characterization of subsurface electric properties, *IEEE Trans. Geosci. Remote Sens.*, *42*, 2555–2568.

Lambot, S., E. C. Slob, M. Vanclooster, and H. Vereecken (2006a), Closed loop GPR data inversion for soil hydraulic and electric property determination, *Geophys. Res. Lett.*, *33*, L21405, doi:10.1029/2006GL027906.

Lambot, S., L. Weihermüller, J. A. Huisman, H. Vereecken, M. Vanclooster, and E. C. Slob (2006b), Analysis of air-launched ground-penetrating radar techniques to measure the soil surface water content, *Water Resour. Res.*, *42*, W11403, doi:10.1029/2006WR005097.

Lambot, S., E. Slob, and H. Vereecken (2007), Fast evaluation of zero-offset Green's function for layered media with application to ground-penetrating radar, *Geophys. Res. Lett.*, *34*, L21405, doi:10.1029/2007GL031459.

Ledieu, J., P. De Ridder, P. De Clercq, and S. Dautrebande (1986), A method of measuring soil moisture by time domain reflectometry, *J. Hydrol.*, *88*, 319–328.

Linde, N., A. Binley, A. Tryggvason, L. B. Pedersen, and A. Revil (2006), Improved hydrogeophysical characterization using joint inversion of cross-hole electrical resistance and ground-penetrating radar traveltime data, *Water Resour. Res.*, *42*, W12404, doi:10.1029/2006WR005131.

Looms, M., A. Binley, K. H. Jensen, L. Nielsen, and T. M. Hansen (2008), Identifying unsaturated hydraulic parameters using an integrated data fusion approach on cross-borehole geophysical data, *Vadose Zone J.*, *7*, 238–248, doi:10.2136/vzj2007.0087.

Lopera, O., E. C. Slob, N. Milisavljevic, and S. Lambot (2007), Filtering soil surface and antenna effects from GPR data to enhance landmine detection, *IEEE Trans. Geosci. Remote Sens.*, *45*, 707–717.

Lunt, I. A., S. S. Hubbard, and Y. Rubin (2005), Soil moisture content estimation using ground-penetrating radar reflection data, *J. Hydrol.*, *307*, 254–269.

Michalski, K. A., and J. R. Mosig (1997), Multilayered media Green's functions in integral equation formulations, *IEEE Trans. Antennas Propag.*, *45*(3), 508–519.

Mualem, Y. (1976), A new model for predicting the hydraulic conductivity of unsaturated porous media, *Water Resour. Res.*, *12*, 513–522.

Nimmo, J. R. (1991), Comment on the treatment of residual water content in "A consistent set of parametric models for the two-phase flow of immiscible fluids in the subsurface" by L. Luckner et al., *Water Resour. Res.*, *27*, 661–662.

Rhoades, J. D., P. A. C. Raats, and R. J. Prather (1976), Effects of liquid-phase electrical conductivity, water content, and surface conductivity on bulk soil electrical conductivity, *Soil Sci. Soc. Am. J.*, *40*, 651–655.

Rhoades, J. D., P. J. Shouse, W. J. Alves, N. A. Manteghi, and S. M. Lesch (1990), Determining soil salinity from soil electrical conductivity using different models and estimates, *Soil Sci. Soc. Am. J.*, *54*, 46–54.

Robinson, D. A., S. B. Jones, J. M. Wraith, D. Or, and S. P. Friedman (2003), A review of advances in dielectric and electrical conductivity measurement in soils using time domain reflectometry, *Vadose Zone J.*, *2*, 444–475.

Rucker, D. F., and T. P. A. Ferré (2004), Parameter estimation for soil hydraulic properties using zero-offset borehole radar: Analytical method, *Soil Sci. Soc. Am. J.*, *68*, 1560–1567.

Slob, E., and J. Fokkema (2002), Coupling effects of two electric dipoles on an interface, *Radio Sci.*, *37*(5), 1073, doi:10.1029/2001RS002529.

Topp, G., J. L. Davis, and A. P. Annan (1980), Electromagnetic determination of soil water content: Measurements in coaxial transmission lines, *Water Resour. Res.*, *16*, 574–582.

Truss, S., M. Grasmueck, S. Vega, and D. A. Viggiano (2007), Imaging rainfall drainage within the Miami oolitic limestone using high-resolution time-lapse ground-penetrating radar, *Water Resour. Res.*, *43*, W03405, doi:10.1029/2005WR004395.

Tsoflias, G. P., T. Halihan, and J. M. Sharp (2001), Monitoring pumping test response in a fractured aquifer using ground-penetrating radar, *Water Resour. Res.*, *37*, 1221–1229.

Vanclooster, M., P. Viaene, J. Diels, and K. Christiaens (1996), WAVE: A mathematical model for simulating water and agrochemicals in the soil and vadose environment, release 2.1, Inst. for Land and Water Manage., Kath. Univ. Leuven, Leuven, Belgium.

van Dam, J. C., J. N. M. Stricker, and P. Droogers (1994), Inverse method to determine soil hydraulic functions from multistep outflow experiments, *Soil Sci. Soc. Am. J.*, *58*, 647–652.

van Genuchten, M. T. (1980), A closed-form equation for predicting the hydraulic conductivity of unsaturated soils, *Soil Sci. Soc. Am. J.*, *44*, 892–898.

Vereecken, H. (1995), Estimating the unsaturated hydraulic conductivity from theoretical models using simple soil properties, *Geoderma*, *65*(1–2), 81–92.

Vereecken, H., J. Maes, J. Feyen, and P. Darius (1989), Estimating the soil-moisture retention characteristic from texture, bulk-density, and carbon content, *Soil Sci.*, *148*(6), 389–403.

Wösten, J. H. M., A. Lilly, A. Nemes, and C. Le Bas (1999), Development and use of a database of hydraulic properties of European soils, *Geoderma*, *90*(3–4), 169–185.

K. Z. Jadoon, S. Lambot, and H. Vereecken, ICG-4 Agrosphere, Institute of Chemistry and Dynamics of the Geosphere, Forschungszentrum Jülich GmbH, D-52425 Jülich, Germany. (k.z.jadoon@fz-juelich.de; s.lambot@fz-juelich.de; h.vereecken@fz-juelich.de)

E. Slob, Department of Geotechnology, Delft University of Technology, Stevinweg 1, NL-2628 CN Delft, Netherlands. (e.c.slob@tudelft.nl)

M. Vanclooster, Department of Environmental Sciences and Land Use Planning, Université Catholique de Louvain, Croix du Sud 2 Box 2, B-1348 Louvain-la-Neuve, Belgium. (marnik.vanclooster@uclouvain.be)